Journal of
Nanoscience and Nanotechnology
Vol. 9, 6600–6605, 2009

# Properties of Mechanochemically Synthesized ZnS Nanoparticles

E. Dutková[1,*], P. Baláž[1], P. Pourghahramani[2], S. Velumani[3], J. A. Ascencio[4], and N. G. Kostova[5]

[1] Institute of Geotechnics, Slovak Academy of Sciences, 043 53 Košice, Slovakia
[2] Mining Engineering Department, Sahand University of Technology, P.O. Box 51335/1996, Tabriz, Iran
[3] Department of Physics, TEC de Monterrey–Campus Monterrey, Monterrey, Nuevo Leon, C.P. 64849, Mexico
[4] Instituto Mexicano del Petróleo, Col San Bartolo Atepehuacan. D.F., C.P. 07730, México
[5] Institute of Catalysis, Bulgarian Academy of Sciences, 1113 Sofia, Bulgaria

The bulk and surface properties of mechanochemically synthesized ZnS nanoparticles were studied. XRD, SEM, TEM (HRTEM), AFM, UV-VIS, low temperature nitrogen sorption as well as TPR characterization methods have been applied. Cubic ZnS nanocrystals (2–4 nm) with characteristic blue shift have been obtained by high-energy milling. There is an evidence of the nanocrystal aggregates formation in products of milling. The surface uniformity, homogeneity as well as enhanced uptake of hydrogen have been documented.



**Keywords:** Zinc Sulphide, Nanoparticle, Mechanochemistry, Synthesis.

## 1. INTRODUCTION

Nanoparticles are distinguished from bulk due to the high surface to volume ratio that causes the structural and electronic changes, which in turn, induce other properties to become different from that of the bulk. Unique photophysical, photochemical, photoelectronic, and photocatalytic properties can occur in semiconductor nanoparticle systems. The differences can be found at both equilibrium and nonequilibrium states including thermodynamics and kinetics. They critically depend on particle size, shape and surface characteristics. The decrease of particle size leads to an extremely high surface area to volume ratio. This results in an increase in surface specific active sites for chemical reactions and photon absorption to enhance the reaction and absorption efficiency. The enhanced surface area also increases surface states, which changes the activity of electrons and holes, and affects the chemical reaction dynamics.[1]

In recent years, the preparation and characterization of different chalcogenides have attracted considerable attention due to their important unique physical and chemical properties.[2] These properties become specially pointed up if the solids are in nanocrystalline dimensions with grain sizes of about 10 nm. ZnS, as a very important direct wide-bandgap semiconductor material with the highest $E_g$ value (3.66 eV) among all II–VI compounds, has been attracting extensive interest in material science due to its special electronic and optical properties. This semiconductor is used in various applications such as optical coatings, field effect transistors, sensors, transductors and in many other optoelectronic devices such as blue-emitting diodes, electroluminescence devices and solar cells.[3] Therefore, much research on ZnS particles and their physicochemical properties has been carried out and many methods have been used for the preparation of these nanoparticles[4–9] even as one-dimensional nanostructures[10] in our group.

This paper is focused on study of the properties of ZnS nanoparticles synthesized by a simple mechanochemical route using high-energy milling. Application of this processing route in mechanochemistry leads to preparation of various nanosized particles.[11] The differences in the nanoparticle structure and the corresponding properties become critical when the use of mechanochemical methods is applied, consequently the use of new transmission electron microscopy methods have opened the perspectives to understand clearly the variables that influence properties of the solid under study.[12–15]

## 2. EXPERIMENTAL DETAILS

Mechanochemical synthesis of ZnS nanoparticles was performed in a Pulverisette 6 planetary mill (Fritsch, Germany). The following milling conditions were used—loading of the mill: 50 balls of 10 mm diameter; weight

*Author to whom correspondence should be addressed.


1533-4880/2009/9/6600/006 doi:10.1166/jnn.2009.1361

charge of the total powder mixture in the mill: 14.2 g; ball charge in the mill: 360 g; material of milling chamber and balls: tungsten carbide; rotation speed of the planet carrier: 500 rpm; milling time 5, 10 and 20 minutes using an argon atmosphere as a protective medium in the mill.

The nanoparticles were prepared by high-energy milling of zinc acetate and sodium sulphide mixture according to the reaction

$$(CH_3COO)_2Zn \cdot 2H_2O + Na_2S \cdot 9H_2O \rightarrow ZnS + 2CH_3COONa + 11H_2O \quad (1)$$

The reaction is thermodynamically feasible at ambient temperature, as the enthalpy change is negative. The value $\Delta H^{\circ}_{298} = -171$ kJ mol$^{-1}$ was calculated from thermodynamic data.[16] After the completion of reaction (1) the obtained nanoparticles have been washed, decantated and dried according to the procedure described earlier.[17] The properties of mechanochemically synthesized ZnS(M) were compared with the chemically precipitated ZnS(C) (Fluka, 98%). The XRD measurements were performed by employing an X-ray diffractometer Siemens D5000 bearing Bragg-Brentano geometrical configuration (Siemens, D5000). The X-ray radiation source was a Cu with $\lambda = 1.5406$ Å. Measurements were made for $2\theta$ values over 20–70° in steps of 0.03° with a count time of 5 s. The Profile software supplied by Bruker/Socabin was used in the pattern decomposition (profile fitting) procedures and in the extraction of the parameters. The profile fitting procedure and principles of the methods were discussed in detail in our earlier papers.[18–19] The specific surface area was determined by nitrogen sorption method at liquid nitrogen temperature, using a Gemini 2360 apparatus (Micromeritics, USA). The synthesized samples were analyzed using FE-SEM LEO 1550 scanning microscope in order to investigate the surface morphology of the nanoparticles. Transmission electron microscopic studies were made by applying the high angle angular dark field (HAADF). Low magnification TEM and high resolution TEM (HRTEM-Philips Tecnai 200 operated at 200 kV), have demonstrated to be together an excellent method to study metal sulfide semiconductor nanostructures, where core–shell or stochiometric systems can be distinguished.[20–21] The samples were left uncovered from any conductive material as to keep their original properties. Atomic force microscopy (AFM) analyses were performed using a multi-mode scanning probe microscope (SPM) (Nanoscope IV, Digital Instruments). Temperature-programmed reduction (TPR) was carried out in an apparatus described earlier.[21] A $H_2$–$N_2$ mixture (10 mol% of $H_2$) was used to reduce samples at a flow rate of 17 cm$^3$ min$^{-1}$. The temperature was linearly raised at a rate of 20 °C min$^{-1}$ up to 850 °C. Optical studies were carried out using UV-VIS spectrophotometer HELIOS GAMMA (Great Britain) in the range 200–600 nm in quartz cell by dispersing of synthesized particles in absolute ethanol by ultrasonic stirring.

## 3. RESULTS AND DISCUSSION

The XRD patterns of the chemically precipitated ZnS(C) and mechanochemically synthesized ZnS(M) are shown in Figures 1 and 2, respectively. The XRD analysis of the ZnS(C) confirmed the presence of hexagonal wurtzite, $\alpha$-ZnS (JCPDS 36-1450) and cubic sphalerite, $\beta$-ZnS (JCPDS 5-566). Clearly, the occurrence of a weak reflection peak (200) at 33.4° and a very small peak at 69.9° indicates the cubic phase. In addition, the investigation of the relative intensity and comparison with those in JCPDS database revealed the relatively higher intensities of reflections associated with both phases. However, it should be noted that the wurtzite is the main phase in the sample and only a small amount of sphalerite is present in the ZnS(C).

In contrast, the XRD patterns of the ZnS(M) show mainly the reflections of cubic phase, which is also supported by relative intensity. No reflection peaks was found at 39.6° and 69.9°, which are typical for the hexagonal form. The (200) reflection of the cubic phase at about 33.4° is probably masked due to a large broadening of the reflection (111). The peaks associated with the hexagonal phase disappear with milling and only the cubic structure is evident in the diffraction pattern. The mechanochemical transformation of wurtzite to sphalerite can be attributed to the motion of dislocations in the activated solid. The obtained results agree with the observations of Imamura and Senna.[23] However, Baláž et al. in their preliminary study[17] reported presence of both cubic and hexagonal phases in the product of mechanochemically synthesized ZnS. There are some differences in comparison with the present results which can be caused by non-detailed XRD analysis of XRD patterns owing to the absence of the proper software for XRD evaluation. The higher background on the XRD pattern of ZnS(M) in this work implies the formation of some amorphous material. This X-ray amorphization is frequently observed in mechanochemically treated solids.[11]

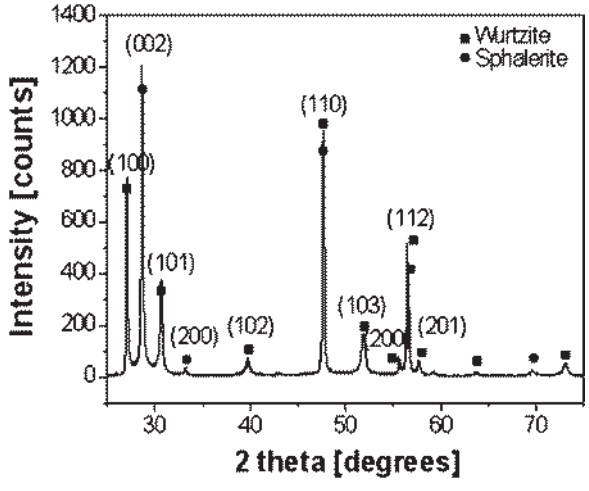


**Fig. 1.** XRD patterns of chemically precipitated ZnS nanoparticles.

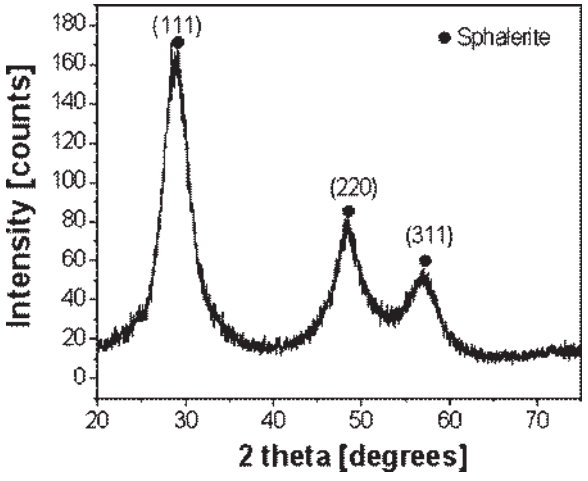


**Fig. 2.** XRD patterns of mechanochemically synthesized ZnS nanoparticles.

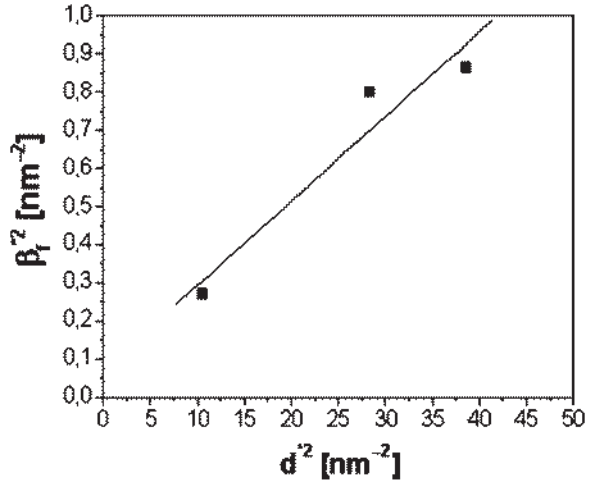


**Fig. 4.** Williamson-Hall plot of mechanochemically synthesized ZnS nanoparticles.



The Williamson-Hall analysis has been applied to ascertain the nature of any structural imperfection in zinc sulphide samples. Figures 3 and 4 show the Williamson-Hall plots for chemically precipitated and mechanochemically synthesized samples, respectively. The scatter of the $\beta_f^{*2}$ values for the ZnS(C) with low correlation coefficient indicates that the crystallite shape differs from a spherical one. In addition, deviation of reflection (102) can be related to the difference in module elasticity between reflection (102) and other reflection. The Williamson-Hall plot yields very small slopes close to zero which implies the precipitated sample is approximately free of strain. For this sample the average volume weighted crystallite size calculated using the intercept of the corresponding lines, is 27.7 nm.

The Warren-Averbach analysis provides detailed information regarding to crystallite size, lattice strain and their distributions. The results of the ZnS(C) using the Warren-Averbach and Scherrer approaches for different reflections are given in Table I. Since the ZnS(C) is free of strain, the Scherrer equation can be applied successfully for calculation of the weighted crystallite size. From the Warren-Averbach method, the average surface weighted crystallite size was estimated as 28 nm, corresponding to the volume weighted crystallite size of 30.5 nm obtained using Scherrer equation. The results gained by the Scherrer equation shows directly good agreement with the results of the Williamson-Hall plots because both the methods measure the volume weighted crystallite size. Hence the obtained results from the Warren-Averbach method and Williamson-Hall plots are comparable.

Regarding the ZnS(M), the presence of non zero slope and intercept reveals that both size and strain components exist in the sample (Fig. 4). The plot shows high correlation coefficient ($r = 0.96$) and negligible scatter in the $\beta_f^{*2}$, suggesting uniform crystallites. The ZnS(M) yields larger broadening compared to the ZnS(C). The volume weighted crystallite size and maximum lattice strain calculated are 3.7 nm and $7.5 \times 10^{-2}$ respectively.

For the ZnS(M) (cubic phase), the Warren-Averbach method was applied to calculate both strain and crystallite size components. The three intensive reflections were used for calculation. The average surface weighted crystallite size obtained was 1.8 nm and the root mean square

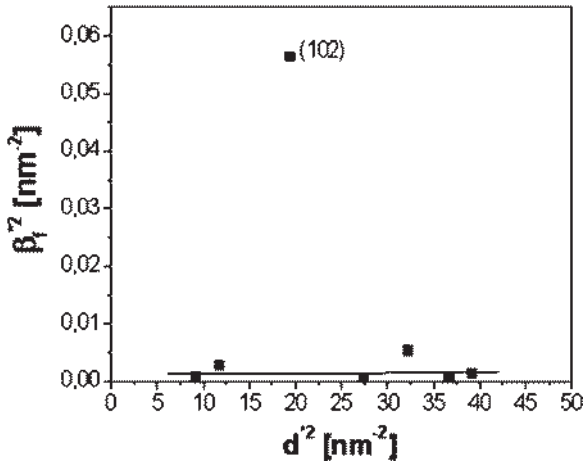


**Fig. 3.** Williamson-Hall plot of chemically precipitated ZnS nanoparticles.

**Table I.** The obtained crystallite sizes for precipitated synthesized ZnS nanoparticles using Warren-Averbach and Scherrer methods.

| Reflections | Scherrer (nm) | Warren-Averbach (nm) |
|---|---|---|
| (100) | 42.0 | 46 |
| (002) | 33.2 | 39.8 |
| (101) | 18.1 | 18.5 |
| (110) | 47.5 | 11.9 |
| (103) | 11.2 | 12.5 |
| (200) | 35.4 | 36.9 |
| (112) | 35.2 | 38.5 |
| (201) | 21.6 | 24.2 |
| Average | 30.5 | 28.5 |
| (102) | 3.7 | 11.5 |

strain (RMSS) at $L = 1$ nm, $\langle \varepsilon^2_{L=1\ \mathrm{nm}} \rangle^{1/2}$, accounted for $2.6 \times 10^{-2}$.

The specific surface area of ZnS(C) which accounts 7 $m^2g^{-1}$ is substantially lower in comparison with ZnS(M) where this value is 97–128 $m^2g^{-1}$ depending on milling time. This increase is related to smaller particles obtained by milling in comparison with surface area of the precipitated sample.

Surface morphology of the ZnS(M) with estimated size from 10–20 nm is depicted in Figure 5(a) showing irregular particles. From the surface analysis it is revealed that there is a homogeneous distribution of the particles and the surface is smooth. Individual nanoparticles have tendency to form nanoparticle agglomerates during milling process and both entities can be clearly seen. In order to analyze the surface characteristics in more detail, sampling methods of AFM in contact mode were used. Figure 5(b) shows a three-dimensional representation of the image obtained from the surface of the ZnS(M) nanoparticles. A homogeneous distribution of crystalline domains can be observed from the image. The deflection image of the ZnS(M) nanoparticles surface is shown in Figure 5(c), from which the crystalline distribution was observed to be uniform and regular. From the comparison of the deflection image (Fig. 5(c)) and the altitude topography (Fig. 5(b)) it is observed that the crystallites were of the same size. We obtained the information from the sample surface, which is shown in Figure 5(c), where the effect of homogeneity is proportional to the altitude information.

Moreover, the way how the material is produced can be studied from the local analysis of the produced aggregates. In this way, HAADF signal gives information about Zn contrast. In Figure 6, a TEM analysis help us to identify regions with pure zinc or sulphur, or homogeneous ZnS distribution. In the bright field image (Fig. 6(a)) the morphology looks like an aggregate produced by smaller clusters compacted during milling, which in case of the HAADF image (Fig. 6(b)) shows that the different wideness with multiple internal boundaries and aparently homogeneous appearance are contrasting. A higher magnification of the zone (Fig. 6(c)) allows recognizing the differences between the contrast produced by the wideness of the aggregate and the homogeneity produced by the similar elemental composition of the material. In this way, the material is determined as homogeneous ZnS aggregates. While the corresponding structural analysis requires

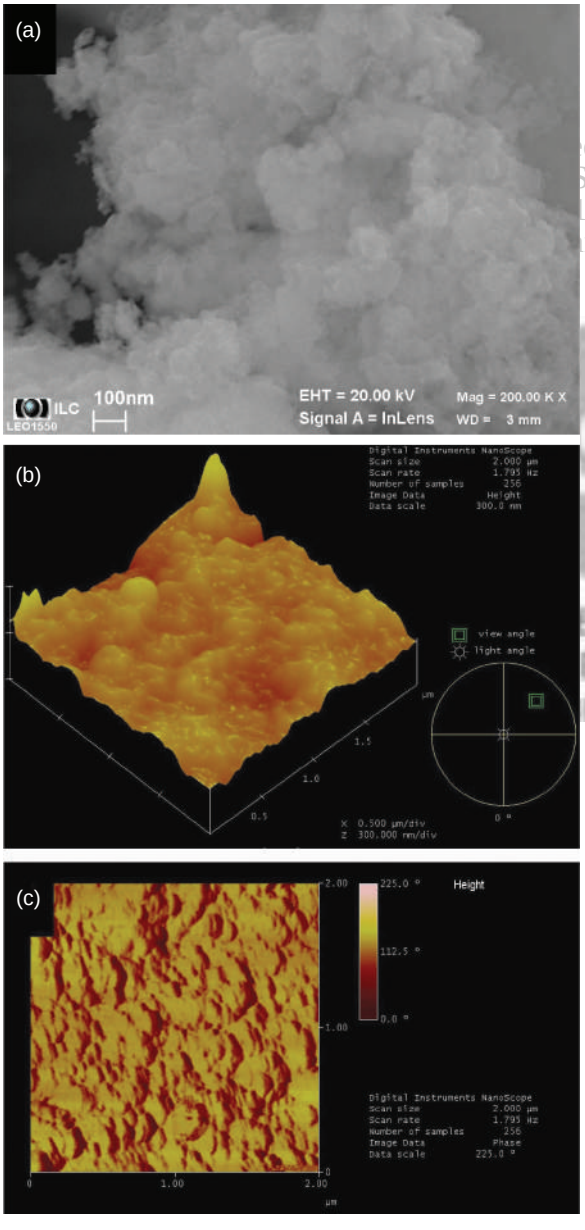


**Fig. 5.** Microscopic analysis of mechanochemically synthesized ZnS nanoparticles by SEM (a), and AFM evaluating the height by a 3D image (b) and the homogeneity with a deflection-mode image (c).

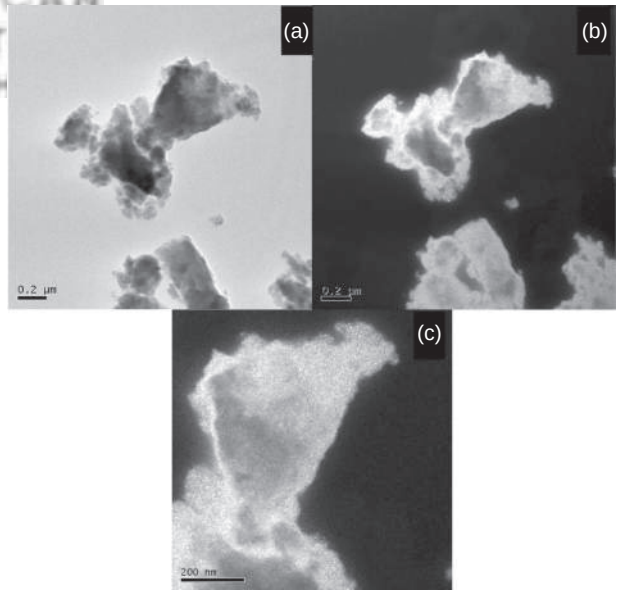


**Fig. 6.** TEM analysis of mechanochemically synthesized of ZnS nanoparticles: (a) bright field, (b) HAADF and (c) higher magnification HAADF images.

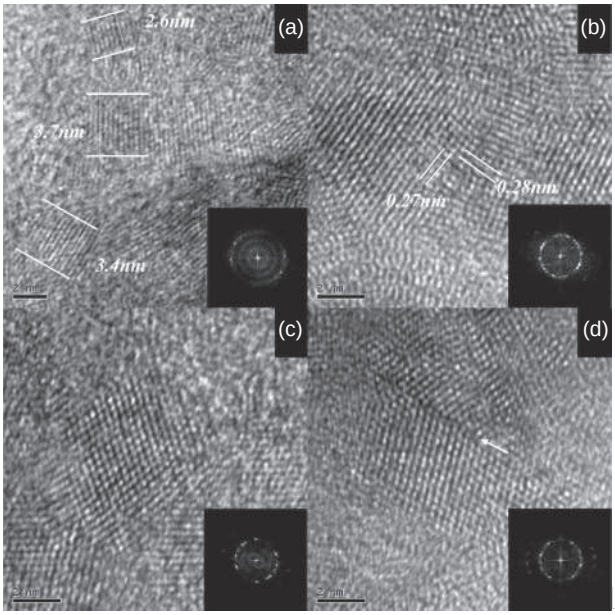


**Fig. 7.** HRTEM analysis of mechanochemically synthesized ZnS nanoparticles: (a) identification of nanoparticle with size around 3 nm, (b) determination of structure with help of the interplanar distance measurement, (c) hexagonal profiles for fcc-like nanoparticles and (d) example of fractures induced in the material.

a higher resolution, the HAADF allows to conclude the formation of ZnS nanocrystals.

HRTEM images allows the determination of size of the nanoparticles,[24] the type of structures produced[25] and also the possible induced morphologies.[26] In Figure 7 four different micrographs are shown. In Figure 7(a) an area of 16 nm × 16 nm is observed, where several clusters are clearly identified, and particularly three of them are measured with sizes of 2.6, 3.7 and 3.4 nm. In fact the corresponding fast Fourier transform (FFT) denotes a polycrystalline material, which must be composed by the nanocrystals. Higher magnification allows determining the lattice distance of the material as in case of Figure 7(b), where it is found a square contrast in the center of the micrograph with interplanar distances of 0.27 and 0.28 nm that implies a region with an axis zone near to the [0, 0, 1]. Figure 7(c) shows a well defined cluster of ∼4 nm with an hexagonal profile and rhombic internal contrast that are characteristic of a truncated octahedron particle observed in the [0, 1, 1] zone axis. The HRTEM images allow finding defects in the nanocrystalline material as marked with an arrow in Figure 7(d), which have been reported for the mechanosynthesized nanostructures.[11]

Temperature-programmed reduction (TPR) patterns of the ZnS(M) and ZnS(C) in Figure 8 consist of four reduction stages with maxima at 390, 465, 585 and 775 °C which could be ascribed to the reduction of zinc sulphide with different dispersion and reducibility. The $H_2$ consumption on the ZnS(M) (3.141 Mmol $H_2$ $g^{-1}$) is 3-times higher in comparison with the ZnS(C) (1.325 Mmol $H_2$ $g^{-1}$). Most probably it is related to the increase of specific surface area as well as to the very active centers on surface of ZnS(M) created by milling. The TPR results show that the ZnS(M) is reduced substantially easily comparing to the ZnS(C).

The UV-VIS optical absorption spectrum of the ZnS(M) nanoparticles is shown in Figure 9. The spectrum is distinctly different compared to the well-known featureless absorption edge of bulk ZnS that appears approximately at 340 nm. The spectrum is structured with the absorption maximum at 309 nm. Compared with that of the bulk ZnS ($E_g = 3.66$ eV), the corresponding band gap of nanosized ZnS(M) is 3.99 eV with the blue shift about 0.33 eV.[27] This can be explained as a quantum size effect, due to electron–hole confinement in a small volume. It is clear from the experimental spectrum that there is a large shift of the absorption maximum of the ZnS(M) towards shorter wavelength. The relation between this shift and the crystallite size is defined by Brus equation.[28] According



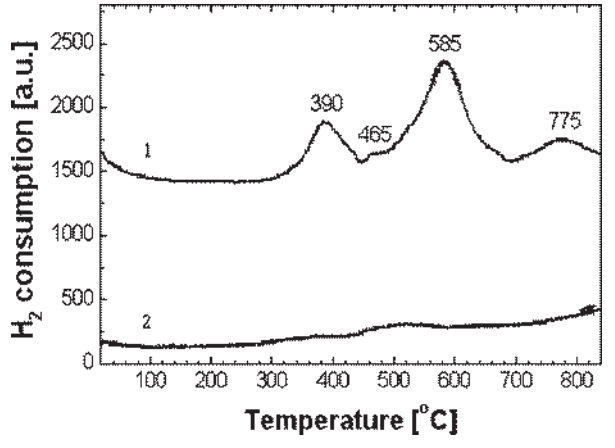


**Fig. 8.** TPR patterns of mechanochemically synthesized (1) and precipitated (2) ZnS nanoparticles.

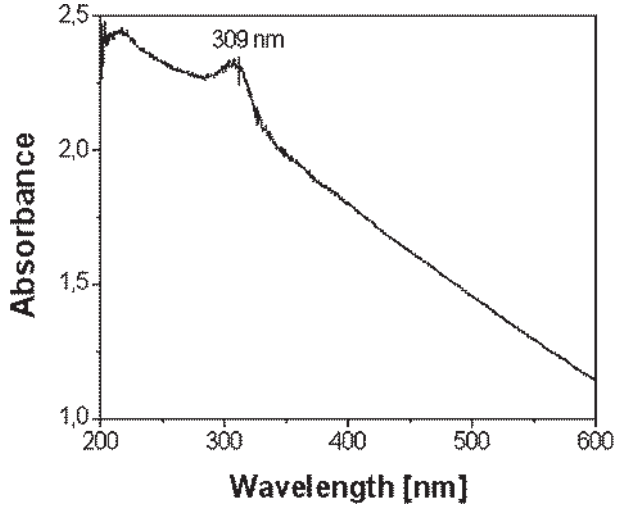


**Fig. 9.** UV-VIS spectrum of mechanochemically synthesized ZnS nanoparticles.

to this equation we calculated the crystallite size 2.1 nm which is in a good agreement with XRD and HRTEM analysis.

## 4. CONCLUSIONS

ZnS nanoparticles of size 2–4 nm have been successfully synthesized by mechanochemical route in the planetary mill. The cubic structure for the peaks associated to (111), (220) and (311) planes were clearly identified. The mechanochemically synthesized ZnS nanoparticles in comparison with chemically synthesized ZnS are distinguished by their physicochemical properties. The main advantages of mechanochemical synthesis is the production of uniform crystallites compared with precipitation chemical route. The absorption spectrum showed a blue shift compared with that of the bulk material indicating its quantum confinement. Investigation by microscopy methods also revealed the surface uniformity and homogeneity of mechanochemically synthesized nanoparticles. Mechanochemical synthesis of ZnS nanoparticles is an alternative solid-state way to prepare nanostructures. The process is solvent-free, does not need high temperatures and long reaction times and is able to manufacture nanomaterials at capacities of ten kilograms per hour.

**Acknowledgment:** The support through the Slovak Grant Agency VEGA (grant 2/0035/08), the Slovak Research and Developing Agency APVV (0347-06), Center of Excellence of Slovak Academy of Sciences NANOSMART and International Laser Center (ILC) in Bratislava (SEM measurements) is gratefully acknowledged. We appreciate the help extended by Dr. Ramiro Perez Campos for the HRTEM analysis. We acknowledge the support extended by the research chairs on Energy and Nanomaterials at TEC de Monterrey-campus Monterrey.



## References and Notes

1. J. Z. Zhang, *J. Phys. Chem. B* 104, 7239 (**2000**).
2. K. J. Klabunde, Nanoscale Materials in Chemistry, Wiley Interscience, New York (**2001**).
3. Ch. Lan, K. Hong, W. Wang, and G. Wang, *Solid State Commun.* 125, 455 (**2003**).
4. P. Baláž, M. Bálintová, Z. Bastl, J. Briančin, and V. Šepelák, *Solid State Ionics* 101, 45 (**1997**).
5. S. A. Chen and W. M. Liu, *Langmuir* 15, 8100 (**1999**).
6. N. A. Dhas, A. Zaban, and A. Gedanken, *Chem. Mater.* 11, 806 (**1999**).
7. L. P. Wang and G. Y. Hong, *Mater. Res. Bull.* 35, 695 (**2000**).
8. N. R. Pawaskar, S. D. Sathaye, M. Bhadbhade, and K. R. Patil, *Mater. Res. Bull.* 37, 1539 (**2002**).
9. J. Chen, Y. Li, Y. Wang, J. Yun, and D. Cao, *Mater. Res. Bull.* 39, 185 (**2004**).
10. S. Velumani and J. A. Ascencio, *Appl. Phys. A* 79, 153 (**2004**).
11. P. Baláž, Extractive Metallurgy of Activated Minerals, Elsevier, Amsterdam (**2000**).
12. R. Esparza, J. A. Ascencio, G. Rosas, J. F. Sánchez Ramirez, U. Pal, and R. Perez, *J. Nanosci. Nanotechnol.* 5, 641 (**2005**).
13. G. Rosas, R. Esparza, H. B. Liu, J. A. Ascencio, and R. Perez, *J. Nanosci. Nanotechnol.* 5, 2133 (**2005**).
14. G. Rosas, R. Esparza, H. B. Liu, J. A. Ascencio, and R. Pérez, *Mater. Lett.* 61, 860 (**2007**).
15. G. Rosas, J. A. Ascencio, A. Medina, and R. Perez, *Appl. Phys. A* 80, 377 (**2005**).
16. D. D. Wagman, W. H. Evans, V. B. Parker, R. H. Schumm, I. Halow, S. M. Bailey, K. L. Churney, and R. L. Nuttall, *J. Phys. Chem. Ref. Data* 11, 392 (**1982**).
17. P. Baláž, E. Boldižárová, E. Godočíková, and J. Briančin, *Mater. Lett.* 57, 1585 (**2003**).
18. P. Pourghahramani and E. Forssberg, *Int. J. Miner. Process.* 79, 106 (**2006**).
19. P. Pourghahramani and E. Forssberg, *Int. J. Miner. Process.* 79, 120 (**2006**).
20. U. Pal, P. Santiago, J. Chavez, and J. A. Ascencio, *J. Nanosci. Nanotechnol.* 5, 609 (**2005**).
21. F. Paraguay-Delgado, W. Antunez-Flores, M. Miki-Yoshida, A. Aguilar-Elguezabal, P. Santiago, J. R. Díaz, and J. A. Ascencio, *Nanotechnology* 16, 688 (**2005**).
22. O. Šolcová, Ch. D. Uecker, U. Steinike, and K. Jirátová, *Appl. Catal. A* 94, 153 (**1994**).
23. K. Imamura and M. Senna, *Mater. Res. Bull.* 9, 59 (**1984**).
24. M. José-Yacamán, J. A. Ascencio, and H. Liu, *J. Vac. Sci. Technol. B* 19, 1091 (**2001**).
25. J. A. Ascencio, C. Gutiérrez-Wing, M. E. Espinosa-Pesqueira, M. Marín, S. Tehuacanero, C. Zorrilla, and M. José-Yacamán, *Surf. Sci.* 396, 349 (**1998**).
26. J. S. Ascencio, H. B. Liu, U. Pal, A. Medina, and Z. L. Wang, *Microsc. Res. Techniq.* 69, 522 (**2006**).
27. N. A. Dhas, A. Zaban, and A. Gedanken, *Chem. Mater.* 11, 806 (**1999**).
28. L. E. Brus, *J. Chem. Phys.* 80, 4403 (**1984**).

Received: 7 March 2007. Accepted: 15 January 2009.